Effects of Beamforming Techniques on Quality of Ultrasound Computed Tomography Images

Razieh Solgi[1,2], Hossein Ghadiri[3,4]*

[1]MSc, Department of Medical Physics and Biomedical Engineering, Tehran University of Medical Sciences, Tehran, Iran
[2]MSc, Preclinical Lab, Core Facility, Tehran University of Medical Sciences, Tehran, Iran
[3]PhD, Department of Medical Physics and Biomedical Engineering, Tehran University of Medical Sciences, Tehran, Iran
[4]PhD, Advanced Medical Technologies and Equipment Institute, Research Center for Molecular and Cellular Imaging, Tehran University of Medical Sciences, Tehran, Iran

ABSTRACT

Background: In body tissues, tumors generally have different speeds of sound (SOS) than normal tissues. In this respect, ultrasound computed tomography (UCT) can generate a cross-sectional SOS map as an innovative ultrasound imaging method. This technique can produce images with a resolution of millimeters and a high signal-to-noise ratio.

Objective: This study aimed to improve UCT image quality without increasing breast cancer screening and diagnosis time.

Material and Methods: In this analytical study, a ring-shaped UCT breast imaging system was simulated using the K-wave toolbox of MATLAB. The system has a 20 cm diameter and 256 ultrasonic piezoelectrics placed in the ring's circumference. Different beamforming techniques imaged two designed phantoms (i.e., resolution and contrast), and the resolution and contrast to noise ratio (CNR) were calculated.

Results: The results of resolution phantom imaging without any beamforming showed that only bars with the value of 0.125 and 0.167 lp/mm were distinguishable, and the 0.1 bars were not recognizable in the imaging. In addition, increasing the number of transmitters led to no noticeable change in resolution for 0.125 and 0.167 lp/mm bars. In all beamforming techniques for imaging the contrast phantom, the CNR parameter up to an object with a diameter of 8 mm increases with increasing diameter without any change.

Conclusion: The beamforming technique using three simultaneous transmitters improved the resolution by about 1 mm compared to the normal strategy. In addition to high-contrast images, beamforming with 9 simultaneous transmitters led to a preferable technique.

Citation: Solgi R, Ghadiri H. Effects of Beamforming Techniques on Quality of Ultrasound Computed Tomography Images. *J Biomed Phys Eng*. 2022;12(4):349-358. doi: 10.31661/jbpe.v0i0.2107-1367.

Keywords

Beamforming; Fan Beam Back Projection; Image Quality Enhancement; Image Reconstruction; Ultrasound Computed Tomography; Ultrasound Imaging; Signal-To-Noise Ratio; Ultrasonography; Tomography

Introduction

X-ray mammography, magnetic resonance imaging (MRI), and ultrasound are common techniques used to detect breast cancer. Although X-ray mammography is the standard modality clinically used for breast imaging, this technique is not sensitive enough for dense breast tissue in young women. The ultrasound technique is more sensitive to dense tissue than X-ray mammography and detects more and smaller cancers in dense-breast women [1, 2]. Therefore, many studies have been conducted on automated whole-breast ultrasound scanning systems using the ultrasound computed tomography (UCT) technique

*Corresponding author:
Hossein Ghadiri
Department of Medical Physics and Biomedical Engineering, Tehran University of Medical Sciences, Tehran, Iran
E-mail: h-ghadiri@sina.tums.ac.ir

Received: 17 July 2021
Accepted: 20 October 2021

[3-8]. UCT can provide quantitative images of acoustical parameters, such as speed of sound (SOS), attenuation, and density from measurements of pressure fields [9].

Many modes of acoustic imaging are used, such as diffraction tomography [10], transmission tomography [11-13], and reflection tomography [14-16]; transmission imaging takes SOS, wave imaging, and the attenuation of these waves. UCT imaging in the transmission mode of the breast was actively studied for enhanced tumor detection and characterization [17-21], and many types of reconstruction methods were applied for UCT. Several approaches are considered to reconstruct images from sets of projections [22], such as iterative and filter back projection (FBP) [23]. Since data acquisition with these imaging systems is a long procedure, a more efficient reconstruction method is preferred. The FBP technique is either simpler or faster than the iterative method; therefore, it was selected as the preferred method of reconstruction in this project [24]. The FBP technique works through the direct passage and propagation of rays from materials. We suppose that the ultrasound wave propagates along a straight line and then it will be received by the corresponding receiver element on the opposite side. Different beamforming techniques were established to optimize resolution, contrast, and other image characteristics to investigate the effect of beamforming on ultrasound image quality parameters [24]. Different methods were used to form the beam, such as simultaneous firing or delay-and-sum techniques [25].

This study aimed at investigatin different beamforming methods to identify its best technique for a better image quality in terms of resolution and contrast without increasing the imaging time.

Material and Methods

A. System Simulation

UCT geometry

This analytical study simulated a ring-shaped UCT breast imaging system with a 20-cm diameter equipped with 256 ultrasonic piezoelectrics placed in the ring's circumference. Water temperature was approximately equal to body temperature (37 °C). The central frequency of ultrasonic piezoelectrics was adjusted to 1.5 MHz, and the whole geometry was designed for immersion in the 37 °C water [23]. The elements were uniformly distributed over 360° such that the central angle between two adjacent elements was about 1.4° (Figure 1).

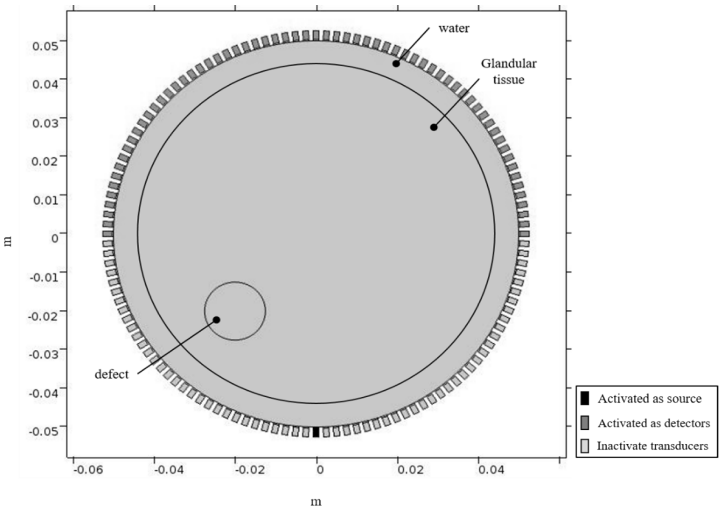

Figure 1: The simulated system, including the piezoelectric elements placed in the circumference of the 20 cm-ring surrounding the water medium and a medium as glandular tissue with a defect immersed

Beamforming method

For each tomographic data acquisition sequence, one piezoelectric (as an ultrasound transmitter) on one side and an opposite semicircle of piezoelectrics on the other side were designed for the receivers (Figure 1). When the first transmitting piezoelectric emitted an unfocused ultrasound wave and all receiving piezoelectrics simultaneously recorded the received signals, the next transmitting piezoelectric was activated; the new opposite semicircle of receiving piezoelectrics repeated the procedure until all piezoelectrics were used as a transmitter.

For stronger signals, a beamforming technique was used in signal transmission. In this technique, a number of piezoelectrics were grouped to send a powerful pulse simultaneously. This study investigated active groups of piezoelectrics, including 3, 5, 7, and 9 transmitters. Figure 2 presents the propagation of waves in the medium for single transmitters, 3, 5, 7, and 9 simultaneous transmitters for the transmitters on the left side. Half of the transmitters' piezoelectrics on the opposite side (Figure 1) acted as receivers in all beamforming.

Simulation method

A 2-D finite difference time domain (FDTD)-based numerical simulation model was developed using commercial simulation k-Wave [26], which is an acoustics toolbox for MATLAB R2016 (MathWorks, Inc., Natick, MA, United States) presenting an advanced time-domain model of acoustic wave propagation. This toolbox with the k-space pseudo-spectral method to solve an acoustic equation reduces simulation memory and time steps [26].

The simulation area included 256 piezoelectric elements surrounding the water medium with an SOS of 1523 m/s and glandular tissue of the beast with an SOS of 1515 m/s (Figure 1). The specifications of the simulation run in this study are shown in Table 1.

The model was subjected to a time-dependent analysis, and such geometry involved contact formulation at the boundary of the tumor. Multiphysics contact problems were often ill-conditioned and might lead to convergence issues for the solver. The solution was extremely sensitive to the contact area and the

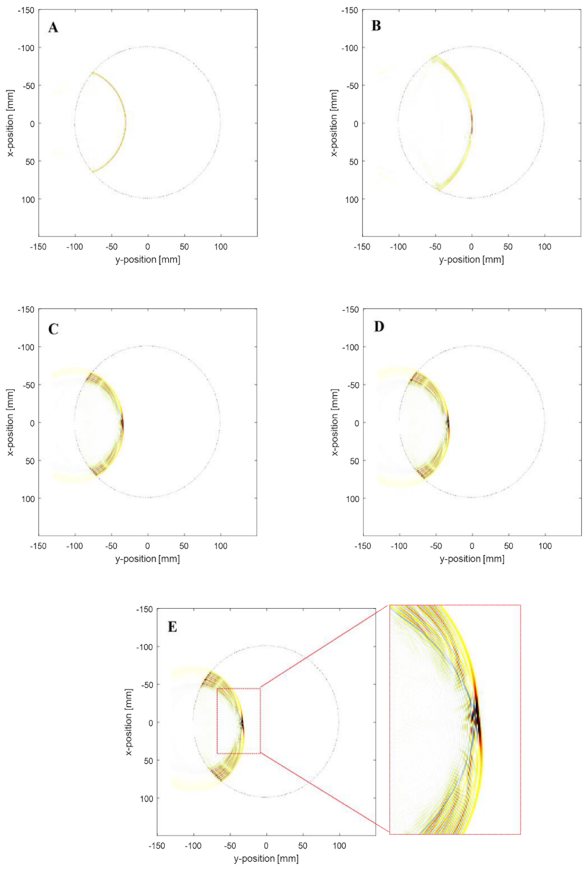

Figure 2: Transmission of wave in the medium by A) single transmitter, B) 3, C) 5, D) 7, and E) 9 simultaneous transmitters microsecond after the transmit pulse (the active piezoelectrics are placed at left)

Table 1: Simulation specifications of the ultrasound computed tomography (UCT) system

UCT system specifications	value
Frequency	1.5 MHz
Number of piezoelectric	256
Piezoelectric array diameter	20 cm
Water bath temperature	37 °C

UCT: Ultrasound computed tomography

mesh size. In other words, if a very small target was placed in the medium and simulation area, an extra-fine mesh was necessary; accordingly, a sufficiently large contact area was used with a normal-sized physics-controlled mesh. The mesh size was considered according to the short acoustic pulse resolve. All Calculations were done based on a computational grid with a 0.5 mm grid point size (the Nyquist limit of two grid points per wavelength) [27]. In addition, an absorption layer was defined around a computational grid with a thickness of 0.92 cm for absorbing the acoustic waves when they reached the edges of the computational domain. This technique can lead to avoiding any computational domain reflections.

B. Time of Flight (TOF) Calculation

In this study, only the first pulse of each received acoustic signal, corresponding to the directly transmitted wave, was used in the computations. According to Figure 3, the time-of-flight (TOF) was the time between the transmitter firing and the time of the first peak of the received signal to each receiver. For any pair of emitting and receiving elements, the TOF of the emitted pulse between the emitter and receiver along the expected straight path can be approximated as:

$$TOF = \sum_i d_i f_i \qquad (1)$$

where d_i is the path length through the i^{th} pixel and f_i is the TOF per unit distance in the i^{th} pixel.

By firing a transmitter, the semicircle of piezoelectrics on the opposite side acted as a receiver. The numbers of piezoelectric elements and receivers in the current simulated system were 256 and 129, respectively. The computation of the TOF between a transmitter and all receivers led to a line of image sinogram. Afterward, the TOF sinogram was completed by firing all the 256 piezoelectrics and calculating the TOF for each transmitter and receiver (Figure 3).

C. Phantom study

Resolution Phantom design

In this step, a resolution phantom was designed, including different spatial frequencies of 0.1, 0.125, and 0.167 lp/mm. The phantom bars were designed to act similar to a 1000 m/s SOS material; the bars were housed in a medium with 1515 m/s SOS as the glandular tissues were immersed in a 37 °C-water with the SOS of 1523 m/s. Such a phantom was designed to compare our simulated system with a typical commercialized breast UCT (i.e., CURE (designed and built at the Karmanos Cancer Institute (KCI), Detroit, MI, USA) [23]. According to the results of the CURE system, its resolution in the transmission mode was 4 mm, corresponding to 0.125 lp/mm. The bars

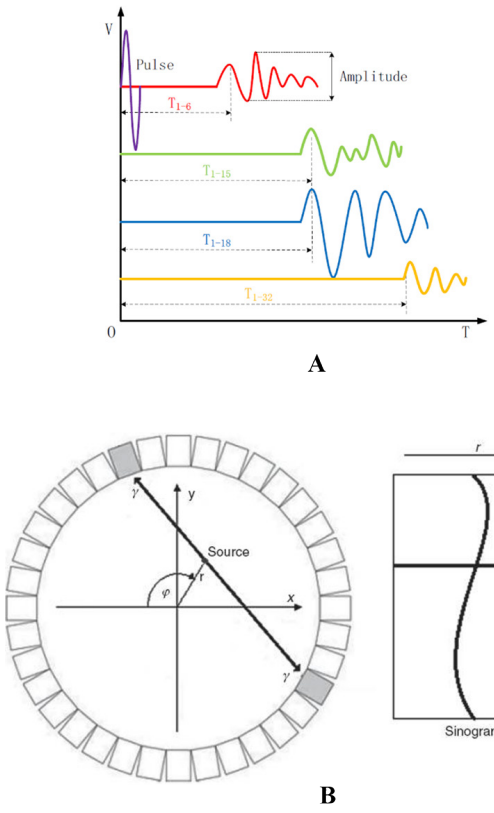

Figure 3: A) The signal of the transmitter and some of the receivers as an example to investigate the Time of Flight (TOF) calculation and B) TOF calculation for each transmitter and receiver to calculate the sinogram

with 0.1 and 0.167 lp/mm, corresponding to 3 mm and 5 mm bars, respectively, were selected to investigate the effect of beamforming techniques on the resolution (Figure 4A).

Contrast Phantom design

In this step, the contrast resolution of the simulated system was characterized by a phantom with an SOS of 1515 m/s (equivalent to the glandular tissue), containing 8 circular objects with diameters of 4-11 mm and the SOS of 1000 m/s in a 37 °C-water bath with SOS of 1523 m/s considered as a contrast phantom in the simulated system (Figure 4B). This system was considered a contrast phantom in the simulated system (Figure 4B).

Image reconstruction

Several image reconstruction methods were applicable in UCT systems [28, 29]; the FBP technique used the Ram-Lack filter for image reconstruction [24]. The TOF images would be calculated by reconstructing the TOF sinogram. Furthermore, according to Equation (1), the SOS images were calculated by pixel size divided into TOF image pixels values.

D. Contrast to noise ratio calculation

The effect of different beamforming techniques on contrast to noise ratio (CNR) was investigated. According to Eq. (2), CNR was defined by dividing the absolute value of the difference between the average light intensity inside the object (S_{obj}) and the average light intensity of the background (S_{bg}) by the standard deviation of it (std_{bg}).

$$CNR = \frac{\left|S_{obj} - S_{bg}\right|}{std_{bg}} \quad (2)$$

Results

Image quality phantoms were used to evaluate the system resolution as well as contrast and investigate the effect of different beamforming techniques on system performance.

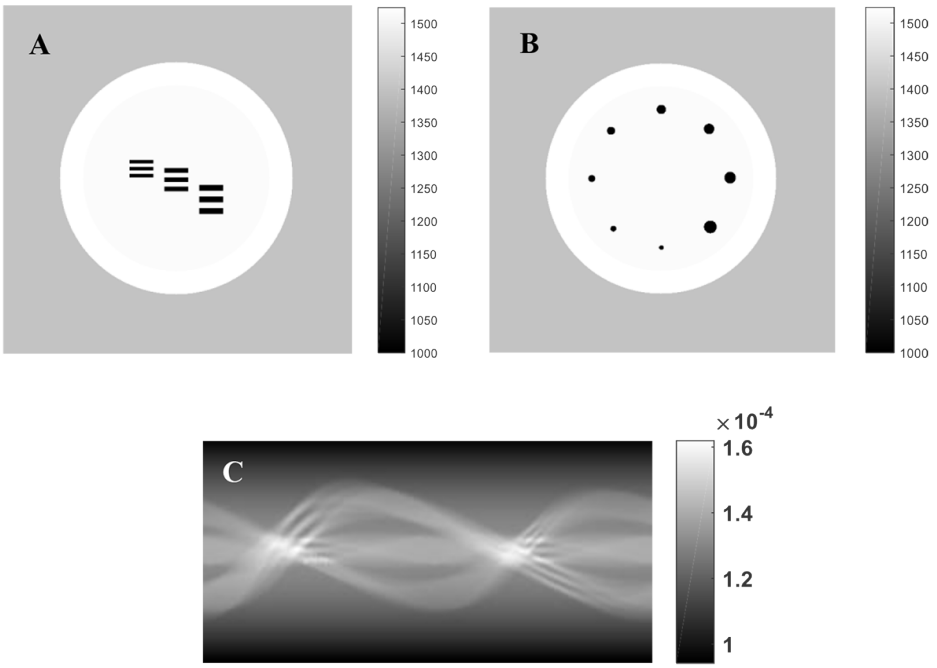

Figure 4: A) Resolution phantom, including different spatial frequencies of 0.1, 0.125, and 0.167 lp/mm in different speeds of sounds (SOSs), from 1000 for bars to 1523 for water, B) contrast phantom contains 8 objects with dimensions of 4 -11 mm with SOS of 1000 m/s, and C) resolution phantom sinogram with a maximum value of 1.6×10^{-4} s and a minimum value of 9.4×10^{-5} s

According to a previous study, the Ram-Lak filter was applied to all sinograms [24].

1) Reconstructed image quality

2) Spatial Resolution

The bar phantom was used with three different values of lp/mm to investigate the system resolution and the effect of beamforming. Figure 5 reveals the images of bar phantom based on different beamforming techniques. The result for bar phantom imaging is shown without any beamforming, in which only the 0.125 and 0.167 lp/mm are distinguishable, and the 0.1 bars are not recognizable in imaging as seen in Figure 5. In addition, Figure 5(B-E) shows the results for imaging with beamforming by 3, 5, 7, and 9 simultaneous transmitters, respectively. According to Figure 5, increasing the number of transmitters leads to no noticeable change in resolution for 0.125 and 0.167 lp/mm bars. A total of 0.1 bars are recognizable by increasing the number of transmitters to 3 and 5. However, in 7 and 9 simultaneous transmitters, the 0.1 bars are not recognizable. The SOS variations are shown by the red lines of 3 mm bars on images in Figure 5(A to E) on 0.1 bars (Figure 5(A to E)).

Figure 5A shows the SOS changes for imaging without beamforming, and the plot shows that the values of bars are near to those of the intra-bars and are not distinguishable. Figures 5B and C show the SOS changes for imaging with beamforming by 3 and 5 simultaneous transmitters. Furthermore, the values of bars and intra-bars are separate enough to distinguish bars. The SOS changes across the 3-mm bars for imaging with beamforming techniques by 7 and 9 simultaneous transmitters are shown in Figures 5D and E, respectively. Finally, the SOS values in the image do not satisfy the actual values in the simulated phantom.

3) Contrast Resolution

Phantom contrast was examined with 8 ob-

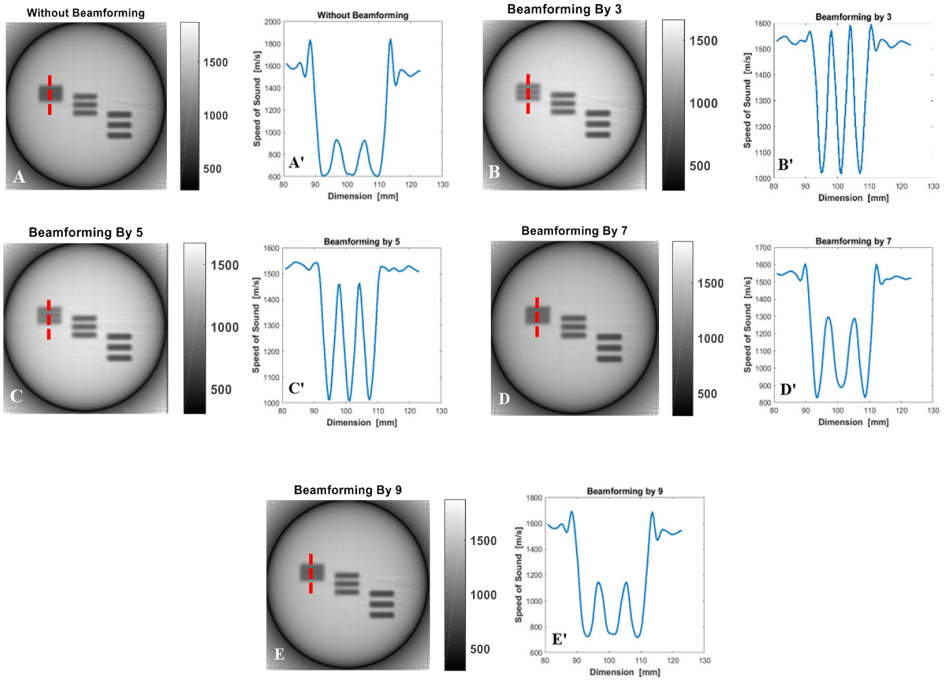

Figure 5: The reconstructed images of resolution phantom by different beamforming techniques using the filter back projection (FBP) method: A) without beamforming, B) beamforming by 3, C) beamforming by 5, D) beamforming by 7, and E) beamforming by 9 and the speeds of sound (SOS) changes across the red line of 3mm bars on images A to E.

jects with different diameters (i.e., 4-11 mm) to investigate the effect of irradiation on contrast. The reconstruction results of the contrast phantom (Figure 4B) demonstrate that the two objects with 3 mm and 4 mm diameters are not recognizable in all techniques (Figure 6). However, the 5-mm object becomes more recognizable by increasing the number of active piezoelectrics as the source. The CNR parameter is calculated for objects with different dimensions (Figure 7). In all beamforming techniques, increasing the diameter of objects up to 8 mm increases the CNR. The same results are obtained for objects with 9-11 mm diameters. For a fixed object, the CNR increases with increasing the number of simultaneous transmitters.

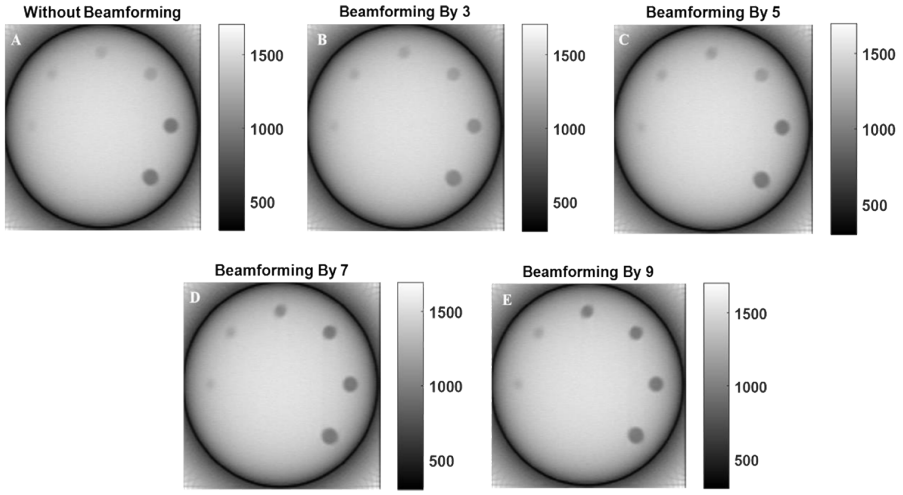

Figure 6: The reconstructed image of contrast phantom by different beamforming techniques through the filter back projection (FBP) method: A) without beamforming, B) beamforming by 3, C) beamforming by 5, D) beamforming by 7, and E) beamforming by 9.

Discussion

Given the importance of UCT systems for high-quality quantitative images and better detection, it is necessary to use some techniques that prevent increasing the imaging time or adding more complexity [30]. The main objective of the present study was to investigate beamforming effects on the resolution and contrast of the images without any delay and summing technique since adding this part would cause the imaging system more complex [31]. This work simulates a UCT system according to the CURE system with similar properties to image resolution and contrast phantoms. Next, it is tried to image them using different beamforming techniques by firing 3, 5, 7, and 9 piezoelectrics simultaneously. Both phantoms are imaged without beamform-

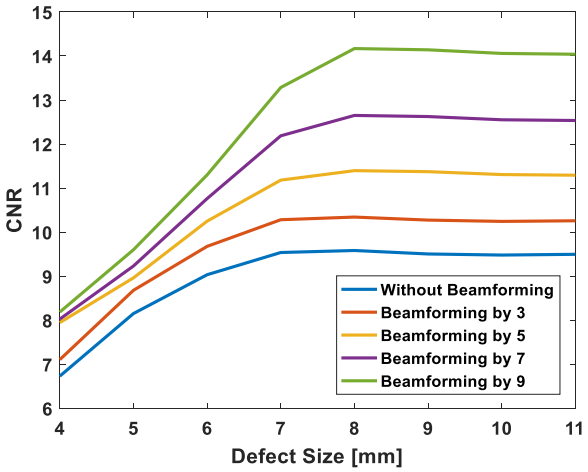

Figure 7: Techniques, the resolution, and contrast to noise ratio (CNR) parameters for objects of different sizes in contrast phantom by applying different beamforming techniques.

ing (with a single transmitter) to simulate the CURE system and compare its result with different beamforming techniques.

According to the results of the CURE system, which provides 4 mm resolution in transmission mode by the FBP reconstruction method [23], it is expected to recognize 4- and 5-mm bars in resolution phantom without applying beamforming technique, confirmed by the present results. However, the 3-mm bars were not recognizable in the single transmitter technique, as expected. By applying beamforming techniques in 3 simultaneous transmitters to image the resolution phantom, the image resolution is improved. A total of 3-mm bars are recognizable in the case of a single transmitter to linear as the propagated beam changes from spherical. Meanwhile, no noticeable change is in resolution with increasing the number of transmitters. This result indicates that the propagated wave is still almost linear up to 5 simultaneous transmitters, and in higher transmitters, it becomes even a point waveform and acts as a virtual source that does not improve the resolution. This result is approved by the comparison between SOS changes across the 3 mm bars in images from different beamforming techniques. A contrast phantom with 8 objects and different diameters was simulated to calculate the CNR, and the results showed that the two objects with diameters of 3 mm and 4 mm were not recognizable in all techniques. The reason is probably that the beam width in all techniques has been larger than the object size. According to the results, increasing the number of active piezoelectrics as a transmitter improves the CNR. For each individual object, the CNR increases with increasing the number of simultaneous transmitters due to increasing the beam energy and decreasing the noise, that beamforming by delay and sum shows the same result [32].

Conclusion

This study shows that beamforming methods affect the image quality in UCT breast imaging systems. The results of this study indicate that the optimal beamforming protocol should be used according to different purposes in imaging. Furthermore, the best CNR can be achieved, and active groups of 9 simultaneous transmitters are selected in the imaging protocol.

Authors' Contribution

R. Solgi performed the simulation and the analysis of the results and wrote the manuscript. H. Ghadiri planned the project and supervised it. The authors read, modified, and approved the final version of the manuscript.

Ethical Approval

The Tehran University of Medical Sciences Ethics Committee approved the study's protocol (Ethic code: IR.TUMS.REC.1394.2025).

Conflict of Interest

None

References

1. Gordon PB, Goldenberg SL. Malignant breast masses detected only by ultrasound. A retrospective review. *Cancer*. 1995;**76**(4):626-30. doi: 10.1002/1097-0142(19950815)76:4<626::aid-cncr2820760413>3.0.co;2-z. PubMed PMID: 8625156.
2. Ying X, Lin Y, Xia X, Hu B, Zhu Z, He P. A comparison of mammography and ultrasound in women with breast disease: a receiver operating characteristic analysis. *Breast J.* 2012;**18**(2):130-8. doi: 10.1111/j.1524-4741.2011.01219.x. PubMed PMID: 22356352.
3. Wiskin J, Borup D, Johnson S, Andre M, Greenleaf J, Parisky Y, Klock J. Three-dimensional nonlinear inverse scattering: Quantitative transmission algorithms, refraction corrected reflection, scanner design and clinical results. Proceedings of Meetings on Acoustics; Acoustical Society of America; 2013.
4. Opieliński K, Pruchnicki P, Gudra T, Podgórski P, Kraśnicki T, Kurcz J, Sąsiadek M. Ultrasound transmission tomography imaging of structure of breast elastography phantom compared to US, CT and MRI. *Archives of Acoustics*. 2013;**38**(3):321-34. doi: 10.2478/aoa-2013-0039.
5. Jiřík R, Peterlík I, Ruiter N, Fousek J, Dapp R,

Zapf M, Jan J. Sound-speed image reconstruction in sparse-aperture 3-D ultrasound transmission tomography. *IEEE Trans Ultrason Ferroelectr Freq Control.* 2012;**59**(2):254-64. doi: 10.1109/TUFFC.2012.2185. PubMed PMID: 24626033.

6. Birk M, Hagner C, Balzer M, Ruiter NV, Hübner M, Becker J. Evaluation of the Reconfiguration of the Data Acquisition System for 3D USCT. *International Journal of Reconfigurable Computing*. 2011. doi: 10.1155/2011/952937.
7. Marmarelis VZ, Jeong J, Shin DC, Do S. High-resolution 3-D imaging and tissue differentiation with transmission tomography. Acoustical imaging; Dordrecht: Springer; 2007. p. 195-206.
8. Fan Y, Wang H, Gemmeke H, Hopp T, Hesser J. Model-data-driven image reconstruction with neural networks for ultrasound computed tomography breast imaging. *Neurocomputing*. 2022;**467**:10-21. doi: 10.1016/j.neucom.2021.09.035.
9. Mamou J, Oelze ML. Quantitative ultrasound in soft tissues. Dordrecht: Springer; 2013.
10. Hemzal D, Peterlík I, Rolecek J, Jan J, Ruiter N, Jiřík R. 3D simulation of diffraction in ultrasonic computed tomography. *Annu Int Conf IEEE Eng Med Biol Soc*. 2008;**2008**:454-7. doi: 10.1109/IEMBS.2008.4649188. PubMed PMID: 19162691.
11. Xiong K, Zhang Y, Zhang Z, Wang S, Zhong Z. PA-NEMO: Proxy mobile IPv6-aided network mobility management scheme for 6LoWPAN. *Elektronika ir Elektrotechnika*. 2014;**20**(3):98-103. doi: 10.5755/j01.eee.20.3.3951.
12. Yinan Q, Tang M, Zhang M. Mass customization in flat organization: The mediating role of supply chain planning and corporation coordination. *Journal of Applied Research and Technology.* 2014;**12**(2):171-81.
13. Jeong JW, Shin DC, Do SH, Blanco C, Klipfel NE, et al. Differentiation of cancerous lesions in excised human breast specimens using multiband attenuation profiles from ultrasonic transmission tomography. *J Ultrasound Med.* 2008;**27**(3):435-51. doi: 10.7863/jum.2008.27.3.435. PubMed PMID: 18314522.
14. Nebeker J, Nelson TR. Imaging of sound speed using reflection ultrasound tomography. *J Ultrasound Med.* 2012;**31**(9):1389-404. doi: 10.7863/jum.2012.31.9.1389. PubMed PMID: 22922619.
15. Birk M, Zapf M, Balzer M, Ruiter N, Becker J. A comprehensive comparison of GPU-and FPGA-based acceleration of reflection image reconstruction for 3D ultrasound computer tomography. *Journal of Real-Time Image Processing*. 2014;**9**(1):159-70. doi: 10.1007/s11554-012-0267-4.
16. Zhang C, Huang L, Zhao Z. Research on combination forecast of port cargo throughput based on time series and causality analysis. *Journal of Industrial Engineering and Management (JIEM)*. 2013;**6**(1):124-34. doi: 10.3926/jiem.687.
17. Littrup PJ, Duric N, Azevedo S, Chambers D, Candy JV, et al. Computerized ultrasound risk evaluation (CURE) system: Development of combined transmission and reflection ultrasound with new reconstruction algorithms for breast imaging. Acoustical Imaging; Boston, MA: Springer; 2002. p. 175-82.
18. Duric N, Littrup PJ, Holsapple E, Babkin A, Duncan R, et al. Ultrasound tomography of breast tissue. Medical Imaging 2003: Ultrasonic Imaging and Signal Processing; San Diego, California, United States: SPIE; 2003. p. 24-32.
19. Carson PL, Meyer CR, Scherzinger AL, Oughton TV. Breast imaging in coronal planes with simultaneous pulse echo and transmission ultrasound. *Science.* 1981;**214**(4525):1141-3. doi: 10.1126/science.7302585. PubMed PMID: 7302585.
20. Gemmeke H, Ruiter NV. 3D ultrasound computer tomography for medical imaging. *Nuclear Instruments and Methods in Physics Research Section A: Accelerators, Spectrometers, Detectors and Associated Equipment.* 2007;**580**(2):1057-65. doi: 10.1016/j.nima.2007.06.116.
21. Schreiman JS, Gisvold JJ, Greenleaf JF, Bahn RC. Ultrasound transmission computed tomography of the breast. *Radiology*. 1984;**150**(2):523-30. doi: 10.1148/radiology.150.2.6691113. PubMed PMID: 6691113.
22. Pérez-Liva M, Herraiz JL, Udías JM, Miller E, Cox BT, Treeby BE. Time domain reconstruction of sound speed and attenuation in ultrasound computed tomography using full wave inversion. *The Journal of the Acoustical Society of America.* 2017;**141**(3):1595-604. doi: 10.1121/1.4976688.
23. Duric N, Littrup P, Poulo L, Babkin A, Pevzner R, et al. Detection of breast cancer with ultrasound tomography: first results with the Computed Ultrasound Risk Evaluation (CURE) prototype. *Med Phys.* 2007;**34**(2):773-85. doi: 10.1118/1.2432161. PubMed PMID: 17388195.
24. Solgi R, Gity M, Mahani H, Ghadiri H. Effect of Reconstruction Filters on Ultrasound Computed Tomography Image Quality in Two Different Detector Arrangements: A Preliminary Simulation Study. *Frontiers in Biomedical Technologies.* 2018;**5**(1-2):1-8.
25. Salehnia M, Ghadiri H. Assessment of a Linear Phased Array Transducer Parameters for Brain

Stimulation. *Frontiers in Biomedical Technologies.* 2017;**4**(1-2):1-7.

26. Mast TD, Souriau LP, Liu DL, Tabei M, Nachman AI, Waag RC. A k-space method for large-scale models of wave propagation in tissue. *IEEE Transactions on Ultrasonics, Ferroelectrics, and Frequency Control.* 2001;**48**(2):341-54. doi: 10.1109/58.911717.
27. Treeby BE, Jaros J, Rendell AP, Cox BT. Modeling nonlinear ultrasound propagation in heterogeneous media with power law absorption using a k-space pseudospectral method. *J Acoust Soc Am.* 2012;**131**(6):4324-36. doi: 10.1121/1.4712021. PubMed PMID: 22712907.
28. Mahmoudi G, Ghadiri H. Recent Advances in X-Ray CT Image Reconstruction Techniques. *Frontiers in Biomedical Technologies.* 2019;**6**(3):114-6. doi: 10.18502/fbt.v6i3.1693.
29. Mahmoudi G, Fouladi MR, Ay MR, Rahmim A, Ghadiri H. Sparse-view statistical image reconstruction with improved total variation regularization for X-ray micro-CT imaging. *Journal of Instrumentation*. 2019;**14**(8):P08023. doi: 10.1088/1748-0221/14/08/P08023.
30. Jiang X, Xiao Y, Wang Y, Yu J, Zheng H. Plane wave imaging combined with eigenspace-based minimum variance beamforming using a ring array in ultrasound computed tomography. *Biomed Eng Online*. 2019;**18**(1):7. doi: 10.1186/s12938-019-0629-2. PubMed PMID: 30674326. PubMed PMCID: PMC6343295.
31. Lou C, Song J, Zhou L, Peng Y, Ding M, Yuchi M. A fast contrast improved zero-phase filtered delay multiply and sum in ultrasound computed tomography. *Journal of Medical Imaging and Health Informatics.* 2018;**8**(9):1850-4. doi: 10.1166/jmihi.2018.2566.
32. Lou C, Peng Y, Song J, Zhou L, Ding M, Yuchi M. Zero-phase filtered delay multiply and sum in ultrasound computed tomography. *Journal of Medical Imaging and Health Informatics.* 2017;**7**(5):1034-8. doi: 10.1166/jmihi.2017.2133.